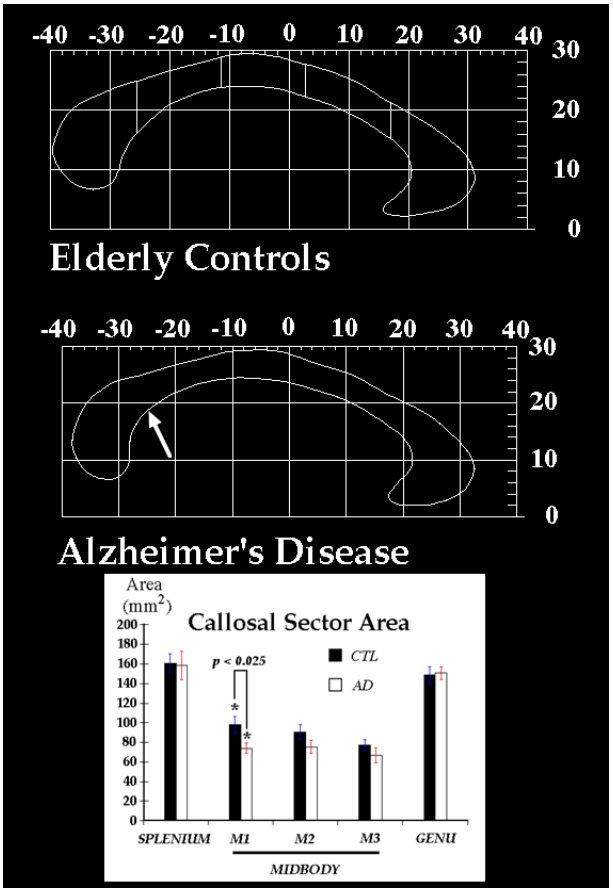

Figure 17.10: Corpus callosum in Alzheimer's disease. Midsagittal corpus callosum boundaries were averaged from patients with Alzheimer's disease and from elderly controls matched for age, educational level, gender, and handedness. The average representations show a focal shape inflection in the Alzheimer's patients relative to normal elderly subjects of the same age. A statistically significant tissue loss is also found at the isthmus (2nd sector, when the structure is partitioned into fifths). The isthmus connects regions of temporo-parietal cortex that exhibit early neuronal loss and perfusion deficits in AD [28, 29].

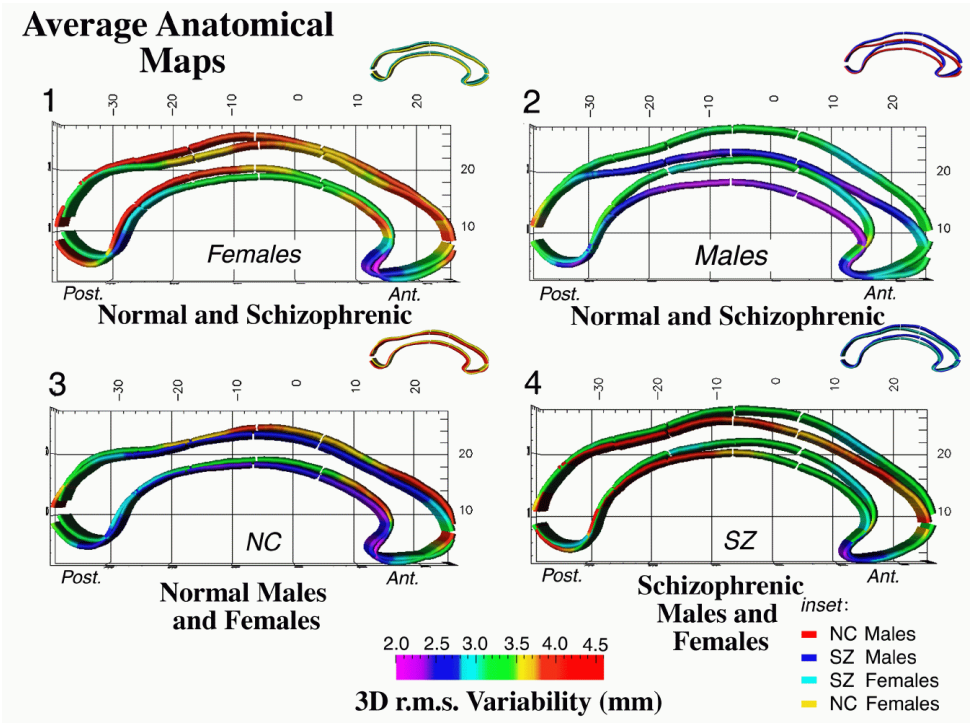

Figure 17.11: Corpus callosum in schizophrenia. (Data from [47]). Midsagittal corpus callosum boundaries were averaged from 25 patients with chronic schizophrenia (DSM-III-R criteria; 15 males, 10 females; age: 31.1±5.6 yrs.) and from 28 control subjects matched for age (30.5±8.7 yrs.), gender (15 males, 13 females), and handedness (1 left-handed subject per group). Profiles of anatomic variability around the group averages are also shown (in color) as an r.m.s. deviation from the mean. Anatomical averaging reveals a pronounced and significant bowing effect in the schizophrenic patients relative to normal controls. Male patients show a significant increase in curvature for superior and inferior callosal boundaries ($p \prec 0.001$), with a highly significant Sex by Diagnosis interaction ($p \prec 0.004$). The sample was stratified by Sex and Diagnosis and separate group averages show that the disease induces less bowing in females (panel 1) than in males (panel 2). While gender differences are not apparent in controls (panel 3), a clear gender difference is seen in the schizophrenic patients (panel 4). Abnormalities localized in a disease-specific atlas can therefore be analyzed to reveal interactions between disease and demographic parameters. (For a color version of this Figure see Plate 33 in the color section of this book.)

underestimated unless elements of the gyral pattern are matched from one subject to another. This matching is also required for cortical averaging; otherwise, corresponding gyral features will not be averaged together. Transformations can therefore be developed that match large networks of gyral and sulcal features with their counterparts in the target brain [18–20, 26, 136, 137]. Differences in cortical organization prevent exact gyrus-by-gyrus matching of one cortex with another. In one approach [25, 26], 38 elements of the gyral pattern are matched, including the major features that are consistent in their incidence and topology across subjects [25, 26, 41, 42, 115, 138, 139].

To find good matches among cortical regions, the matching process can be performed in the cortical surface's parametric space, which permits more tractable mathematics (Figs. 17.12, 17.13). This vector flow field in the parametric space indirectly specifies a correspondence field in 3D, which drives one cortical surface into the shape of another. This mapping not only matches overall cortical geometry, but matches the entire network of the 38 landmark curves with their counterparts in the target brain, and thus is a valid encoding of cortical variation.

17.7.2 Spherical, planar maps of cortex

Several simpler maps of the cortex are made to help calculate the transformation. Cortical models are often created by deforming a spherical mesh into the shape of the cortex [18, 19, 140]. Any point on the cortex then maps to exactly one point on the sphere, and a *spherical map* of the cortex can be made which indexes sulcal landmarks in the normally folded brain surface. These spherical locations, indexed by two parameters, can also be mapped to a plane (Figs. 17.12, 17.13). A flow field is then calculated that elastically warps one flat map onto the other (or equivalently, one spherical map to the other). On the sphere, the parameter shift function $\mathbf{u}(\mathbf{r}) : \Omega \rightarrow \Omega$ is given by the solution $F_{pq} : \mathbf{r} \rightarrow \mathbf{r} - \mathbf{u}(\mathbf{r})$ to a curve-driven warp in the spherical parametric space $\Omega = [0, 2\pi) \times [0, \pi)$ of the cortex [25, 26, 141]. For points $\mathbf{r} = (r, s)$ in the parameter space, a system of simultaneous partial differential equations can be written for the flow field $\mathbf{u}(\mathbf{r})$:

$$L^{\ddagger}\mathbf{u}(\mathbf{r}) + \mathbf{F}(\mathbf{r} - \mathbf{u}(\mathbf{r})) = \mathbf{0}, \forall \mathbf{r} \in \Omega, \quad with \quad \mathbf{u}(\mathbf{r}) = \mathbf{u_0}(\mathbf{r}), \forall \mathbf{r} \in \mathbf{M_0} \cup \mathbf{M_1} \, . \tag{17.23}$$

Here M_0, M_1 are sets of points and (sulcal or gyral) curves where displacement vectors $\mathbf{u}(\mathbf{r}) = \mathbf{u_0}(\mathbf{r})$ matching corresponding anatomy across subjects are known. The flow behavior is modeled using equations derived from continuum mechanics, and these equations are governed by the Cauchy-Navier differential operator $L = \mu\nabla^2 + (\lambda + \mu)\nabla(\nabla\cdot)$ with body force $\mathbf{F}$ [20, 23, 28, 29, 80, 81]. The only difference is that $L^{\ddagger}$ is the $covariant$ form of the differential operator L, for reasons explained next.